Resonant inelastic soft x-ray scattering at double core excitations in solid LiCl

Marcus Agåker,[1] Tanel Käämbre,[2] Chris Glover,[3] Thorsten Schmitt,[4] Maurizio Mattesini,[5] Rajeev Ahuja,[1] Johan Söderström,[1] and Jan-Erik Rubensson[1]

[1]*Department of Physics, Uppsala University, PO Box 530, SE-751 21 Uppsala, Sweden*

[2]*Institute of Physics, University of Tartu, Riia 142 Tartu 51014, Estonia*

[3]*Department of Electronic Materials Engineering, Australian National University, Canberra, ACT, 0200, Australia*

[4]*Paul Scherrer Institut, CH-5232 Villigen PSI, Switzerland*

[5]*Departamento de Física de la Tierra, Astronomía y Astrofísica I, Universidad Complutense de Madrid, E-28040, Spain*

(Received 29 March 2006; published 20 June 2006)

Inelastic soft x-ray scattering in LiCl, resonantly enhanced at states with two Li 1*s* vacancies, is investigated. States in which both excited electrons are localized during the double core hole lifetime, in which one of the electrons delocalize, as well as triply excited states in which the double core excitation is accompanied by a valence-to-conduction band excitation, contribute to the scattering. The angular momentum symmetry of the involved states and the vibronic coupling during the scattering process are reflected in the angular anisotropy. The effect on the local electronic structure of multiple core holes is theoretically studied by means of supercell band calculations.

DOI: 10.1103/PhysRevB.73.245111 PACS number(s): 78.70.Ck, 71.20.−b, 82.80.Ej

I. INTRODUCTION

The term "hollow" applies to atoms with sparsely populated inner shells. Highly correlated hollow states in few-electron systems like the free lithium atom have been a long-standing test bench for advanced atomic theory, and synchrotron radiation has been particularly useful for a detailed characterization of these states and their excitation-decay dynamics.[1] Hollow states *in solids* are normally discussed in another context: as highly charged ions impinge on surfaces,[2,3] the neutralization of the ion creates a highly excited atom with empty inner shells. Electronic and radiative decay of these highly excited states within the solid is used to monitor the charge states, and thereby to gain information about the neutralization process and the general dynamics as the ion enters the material. Due to the complexity of the process, however, no details about the local electronic structure can be learned from this type of experiments.

The radiative decay of states with a double vacancy in the 1*s* orbital leads to so-called hypersatellites[4] in x-ray emission, and in recent years photoexcitation of hollow states in solids[5–7] have been presented in the literature. The excitation-energy dependence of such satellites has been investigated for some metallic systems with fairly heavy elements.[5,6] Generally, the cross section shows a smooth monotonic increase from the onset at threshold, a behavior which has been analyzed in terms of shake-off processes. In contrast to such behavior, strong resonances appear in association with excitation of hollow lithium states in LiCl.[7] A multitude of different states in which both Li core electrons are excited are populated, and can be characterized by monitoring the emitted radiation in the decay as a function of excitation energy. Thus the population of states in which both electrons stay locally at the site of the Li nucleus can be observed, as well as states in which one electron stays localized at the Li nucleus and the other delocalizes before the decay, and triple excitations in which also the valence electrons are involved. These excitations reflect the electronic surrounding and the dynamics at the Li atom site, and hence can potentially be used for chemical analysis. Here we present and discuss an expanded and more detailed data set, aiming at a deeper understanding of these excitations.

II. EXPERIMENT

The measurements were performed at the I511-3 beamline[8] at MAX-lab. This is an undulator beam line with a photon flux at the end-station of approximately 10^{13} photons/s at the used excitation energies (140–150 eV). The modified SX-700 monochromator was set to a resolution of 0.1 eV. The beam was focused on the sample to a spot with a vertical and horizontal full width at half maximum of 20 and 50 μm, respectively, using Kirkpatrick-Baez mounted refocusing mirrors. The intensity of the beam was monitored by recording the photocurrent from a gold mesh inserted into the beam after refocusing optics with a Keithley nanoamperemeter. Partial fluorescence yield (PFY) and energy resolved soft x-ray emission (SXE) spectra were measured using a Gammadata Scienta XES 300 (Ref. 9) grazing incidence Rowland spectrometer. For most of the measurements the XES 300 was mounted to measure the emitted radiation in the direction of the polarization of the incoming radiation (horizontal). For these measurements the spectrometer was operated in slitless mode, in which the entrance slit is removed (i.e., opened to its full extent) and the beam spot is used as source in the spectrometer optics. From the elastically scattered radiation in second order of diffraction, the resolution of the spectrometer was determined to be 0.3 eV. Measurements were also performed with the spectrometer mounted perpendicular to the plane of polarization of the primary radiation (vertical). In this geometry the input slit width was chosen to achieve the same resolving power as in the horizontal mounting. In the PFY mode the XES 300 detector is gated to accept events only in the energy interval of 84–92 eV, and the count rate is recorded as a function of excitation energy.

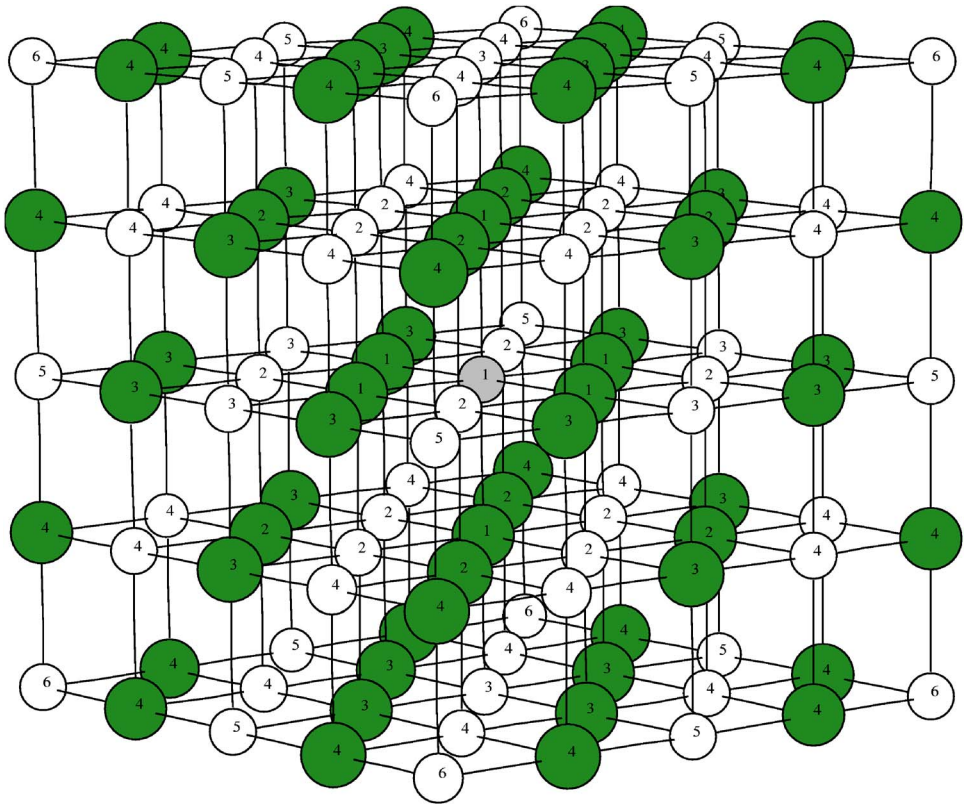

FIG. 1. (Color online) The structure of the LiCl super cell used in calculation. Filled green circles indicate Cl atoms and unfilled are Li atoms. The numbers represent the six lithium sites and four chlorine sites in the cell, and are used as subscripts when the atoms are discussed. Li_1 is the site of the core hole.

The sample was prepared from commercially available LiCl salt grains. These were compressed into a pellet with about 10 mm diameter and 3 mm thickness. This disc was placed in vacuum, mounted on a sample holder. The sample manipulator at the position of measurements is motorized and computer controlled. This enables us to reduce the effects of radiation damage to the sample by moving the sample with regular time intervals, in this case every 10 sec, so that new spots on the sample successively are exposed to the incoming radiation. The homogeneity of the sample was checked by ensuring that the emitted intensity, at constant excitation energy, was the same over the sample-scanning region. The angle between the incoming beam and the sample surface normal was around 60°.

III. THEORY

A. Calculations

In order to interpret the experimental resonant inelastic soft x-ray scattering (RIXS) spectra, first-principles calculations were performed for the cubic LiCl structure ($Fm\bar{3}m$). First, we relaxed the unit-cell volume with an *ab initio* plane-wave program (VASP),[10] where the interaction between the ions and the electrons is described by PW-GGA (Ref. 11) potentials generated within the Blöchl's projector augmented wave (PAW) method.[12] The optimized lattice constant (a =5.1376 Å) was then used in the full-potential linearized augmented plane-wave method (FP-LAPW) (Ref. 13) to compute density of states (DOS) and x-ray-absorption near-edge spectra (XANES). It is worthwhile to note that the relaxed PAW lattice parameter has shown very small residual forces once plugged into the full-potential code. To account for the effect of single ($1s^1$ $2s^1$) and double ($1s^0$ $2s^1$) core holes on the electronic band states, the excited Li atom was formally treated as an impurity in a LiCl supercell of dimension $2\times2\times2$ (Fig. 1) and a background charge was used in order to keep the system neutral. Our model system consists of 32 chlorine ions at four inequivalent sites, and 32 lithium atoms at six different sites. In Fig. 1 the atoms are numbered so that number 1 is the central absorbing atom, and the numbers increase with the distance to this atom for each species. In the following the atoms are referred to this number as subscript.

The FP-LAPW band calculations employed the PW-GGA approximation to describe the exchange correlation potential within density-functional theory (DFT).[14] Atomic sphere radii of 2.42 bohrs were used for both lithium and chlorine. The valence wave functions inside the nonoverlapping muffin-tin spheres were expanded into spherical harmonics up to $l=10$ and the potential up to $l=4$. An APW+local orbital[15] basis set was used with additional local s orbital for all the Li and Cl atoms. Convergence of the calculated spectra with respect to plane-wave expansion parameter $R_{MT}\cdot K_{max}$ and **k**-point sampling was checked. A total of 56 **k** points in the irreducible wedge of the Brillouin zone (BZ) of the cubic supercell and $R_{MT}\cdot K_{max}=7$ was found to be sufficient for getting well converged Li K edges.

Wave function symmetries and angular dependence

Like for the helium atom[16] the interpretation of resonant scattering over double excitations in a free Li^+ ion is simplified by the assumption that dipole selection rules are valid

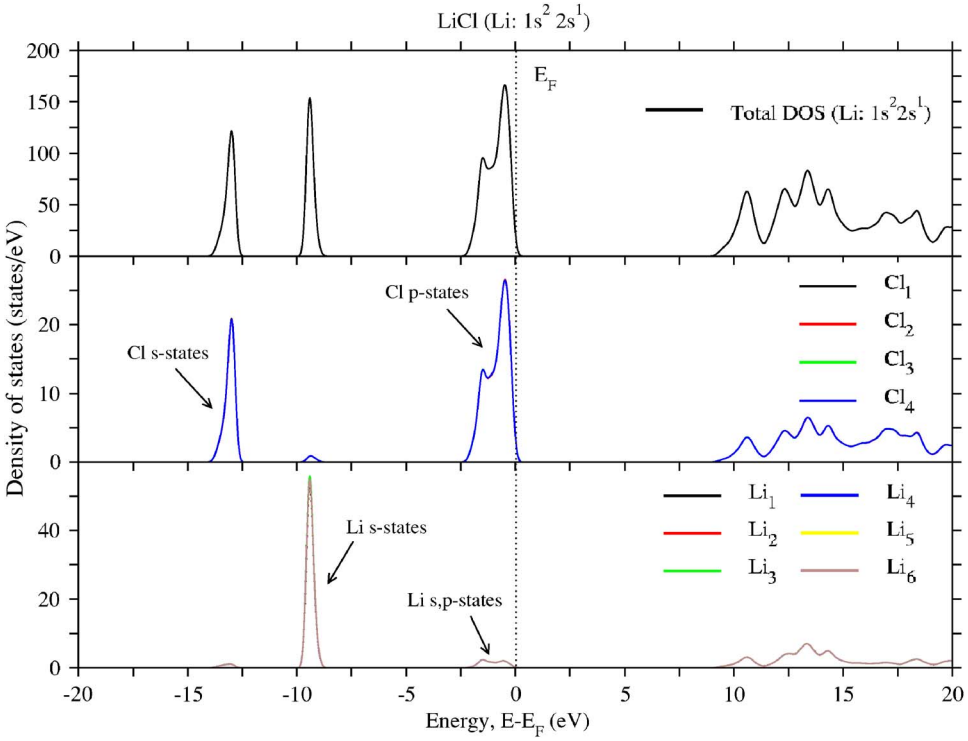

FIG. 2. (Color online) The ground-state density of states projected on the *s*, *p*, and *d* symmetry for the different Li and Cl sites.

and that *LS* coupling applies. Restricting the discussion to doubly excited states where one of the excited electrons is in $n=2$, only

$$1s^2\ {}^1S_0^e \rightarrow 2ln'l'\ {}^1P_1^o \rightarrow 1sn''s\ {}^1S_0^e$$

and

$$1s^2\ {}^1S_0^e \rightarrow 2ln'l'\ {}^1P_1^o \rightarrow 1sn''d\ {}^1D_2^e$$

are possible. Note that the final-state symmetries are complementary to what one gets in direct photoabsorption to singly excited states:

$$1s^2\ {}^1S_0^e \rightarrow 1snp\ {}^1P_1^o.$$

Intermediate states dominated both by $2pns \pm 2snp$ and $2pnd$ configurations may contribute to the scattering. For the corresponding excitations in He it has been demonstrated[16,17] that "$2pnd$" states decay predominantly to ${}^1D$ states, whereas "$2pns$" states decay with large probability both to ${}^1D$ and ${}^1S$ states. We expect this to be similar for the Li^+ ion.

The angular dependence is described by the differential cross section of photon scattering into the solid angle, $d\Omega$:

$$\frac{d\sigma}{d\Omega} = \frac{\sigma}{4\pi}\left(1 + \frac{\beta}{2}(3\cos^2\theta - 1)\right),$$

where σ is the total scattering cross section, θ is the angle between the polarization of the incoming photon and the direction of the outgoing photon, and $\beta=-1$ and $\beta=-0.1$ for ${}^1S$ and ${}^1D$ final states, respectively.[16] The angular resolution of the SXE spectrometer is excellent as it is set by the intrinsically small solid angle of acceptance. Thus assuming perfect horizontal polarization and measuring in the horizontal direction ($\theta=0$) the spectrum gets contributions from ${}^1D$ final states, only ($\sigma_S^{horizontal} \approx 0$ and $\sigma_D^{horizontal} \approx 0.9\frac{\sigma}{4\pi}\Delta\Omega$), whereas in the vertical direction ($\theta=90°$) both ${}^1S$ ($\sigma_S^{vertical} \approx 1.5\frac{\sigma}{4\pi}\Delta\Omega$) and ${}^1D$ ($\sigma_D^{vertical} \approx 1.05\frac{\sigma}{4\pi}\Delta\Omega$) states contribute to the spectrum.

The discussion above concerns the isolated ion. For continuum excitations in a simple cubic broad band solid, on the other hand, we expect scattering to be isotropic. As shown below we indeed observe strong angular anisotropy in the solid, which we assign to quasiatomic behavior. We will use the atomic case as a starting point when discussing the symmetry character of the states involved in the scattering process.

IV. RESULTS AND DISCUSSION

A. Theory: Influence of core vacancies on the local electronic structure

In Figs. 2–4 we show the theoretical predictions of the site- and symmetry-projected local density of states in the ground state (GS), and its changes upon the removal of one and two Li core electrons. In the ground state (Fig. 2) chlorine and lithium states with *s* character appear to be well localized at −13 and −9 eV, respectively. The top of the valence band (VB), near Fermi level, is mainly formed by chlorine *p* states with some admixture of Li *s* and *p* orbitals. The calculated PW-GGA band gap (E_g) amounts to 9.2 eV, which compare quite well with the experimental value of 9.4 eV.[18,19] The bottom of the conduction band (CB) consists of a mixture of empty Li and Cl states of both *s* and *p* character. The bonding type between Li and Cl is clearly ionic, where the Li atoms give fractions of electrons to the surrounding chlorine atoms. As shown in the calculated contour density map of Fig. 5, the electronic ground state of the LiCl crystal is characterized by nondirectional Coulombic interactions.

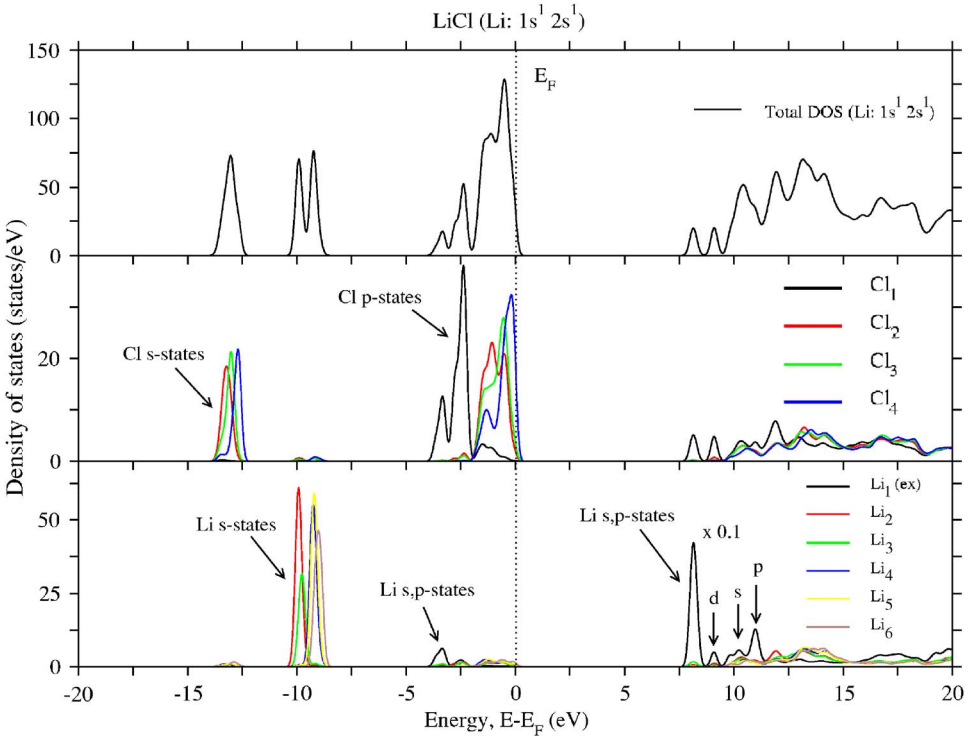

FIG. 3. (Color online) The density of states projected on *s*, *p*, and *d* symmetry in the presence of one core hole for the different Li and Cl sites.

In Fig. 3 the calculated partial DOS of Li_1 with a $1s^1\ 2s^1$ configuration is shown. When removing a 1*s* electron from the central Li atom we observe that the VB states of Li_1 and Cl_1 (i.e., the six atoms constituting the first coordination shell of Li_1) move their barycenter positions downward in energy. Furthermore, Li_1 and Cl_1 show a strong mixing of their *s* and *p* states as indicating a high level of hybridization between the two atoms. Such a kind of electronic *s*,*p* hybridization brings a certain amount of covalent character into the LiCl system that leads to an appreciable band-gap closing (E_g =7.5 eV). In a qualitative way one can say that Pauling's electronegative value of Li_1 becomes as high as that of neighbor Cl_1 ions so that the two species tend to share electrons and to form directional bonds. The bottom of the CB is also dominated by localized empty *s* and *p* states of Li_1 and Cl_1 that have moved downward in energy with respect to the GS case in order to screen the strong 1*s*-hole potential. The charge density plot of Fig. 6(a) further illustrates the changes

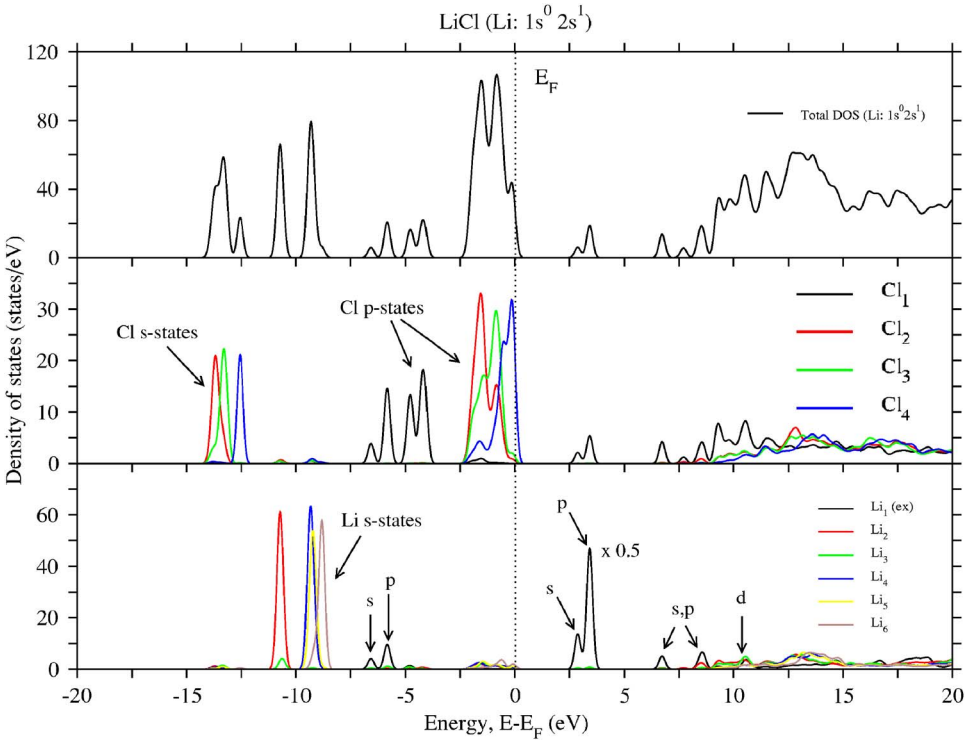

FIG. 4. (Color online) The density of states projected on *s*, *p*, and *d* symmetry in the presence of two core holes for the different Li and Cl sites.

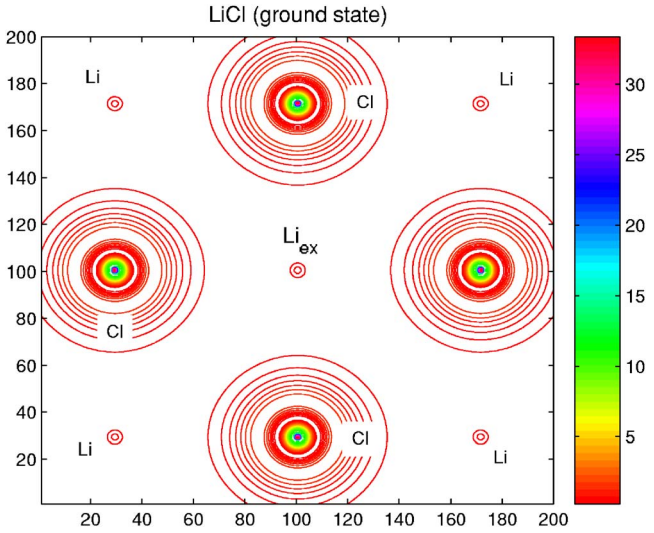

FIG. 5. (Color online) Electron density map for the ground state. The density is expressed in units of (e/Å^3).

in the local electronic structure upon core hole creation. The screening and the polarization of the chlorine atoms constitute an effective charge transfer from the neighbor coordination shells. In particular, the contour lines centered on the Cl_1 atoms are now assuming an elliptical shape, which points to the formation of directional Li_1-Cl_1 bonds. The difference density map [Fig. 6(b)] also shows that Cl_1 atoms have lost electron density (i.e., positive contour lines) with respect to the GS electronic distribution, whilst the central Li_1 atom has gained electron density (i.e., negative contour lines).

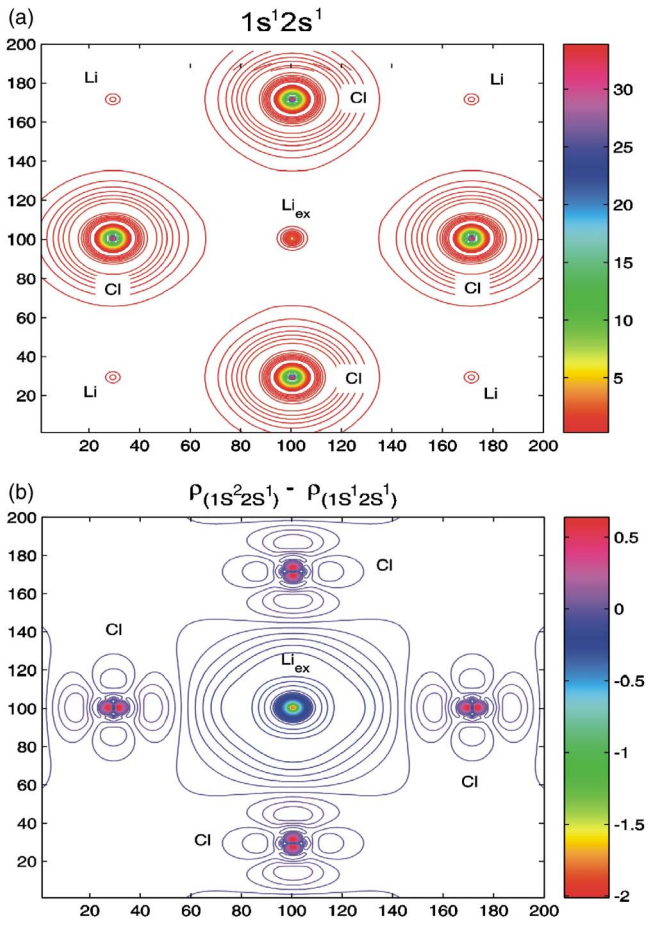

FIG. 6. (Color online) Electron density map in the presence of one core hole on the central Li atom (a), and the difference compared to the ground state (b).

For the case of Li_1 with a $1s^0\,2s^1$ configuration we observed for the partial DOS (Fig. 7) the same trend found for the single core-hole system: the VB is dominated by the strong hybridization between the s and p states of Li_1 and Cl_2, while the bottom of the CB shows localized empty s and p states. The bandwidths of the occupied Li_1 and Cl_1 s and p states increase considerably for the double core-hole system, pointing to a larger hybridization between the central lithium atom and neighbor chlorines. In this case, the calculated energy gap is only 2.5 eV, which is the typical magnitude for semiconductors. The removal of two s electrons from the Li core generates a charged pseudoatom that turns out to be more electronegative than the surrounding chlorines. Therefore the type of Li-Cl bonding around the excited Li site becomes stabilized when the s and p electrons are shared in between the two atomic sites instead of accounting for an effective charge transfer. This development is clearly illustrated in the charge-density plots shown in Figs. 5–7. When removing a second Li core electron [Fig. 7(a)] we find contour lines that are connecting both Li and Cl atoms as to indicate that the system gets more covalent character. Finally, by looking at the intensity of the isolines in the difference density map [Fig. 7(b)] we demonstrate that the absorbing Li atom gains electron density from the surrounding chlorines. This electronic withdrawing to Li_1 from Cl_1 is almost twice as strong as the one found in the case of the single 1s hole.

B. Overview of the experimental results

1. Scattering map

The "equi-intensity" contour diagram in Fig. 8 shows the scattering intensity as a function of excitation energy (E_1) on the vertical axis, and of emission energy (E_2) on the horizontal axis. The map is constructed from 68 SXE spectra, excited at different excitation energies in the region of the resonances. The PFY spectrum, shown to the right in Fig. 8, monitors the integrated emission intensity in the emission-energy region where the main emission features are found (84–92 eV) as a function of excitation energy. Diamonds in the PFY represent the integrated intensity for each SXE spectrum over the given energy range.

Compared to the first observations of the double excitations in LiCl reported in Ref. 7, the current data set presents a considerable improvement. We can now investigate the excitations in detail. We start the discussion by assigning the main features in the emission map, an assignment which is in full accordance with Ref. 7.

2. Calibration and artifacts

The SXE spectra are measured in a grazing incidence spectrometer in which the radiation is diffracted by the grating in several orders. The dots in the diagonal line of inten-

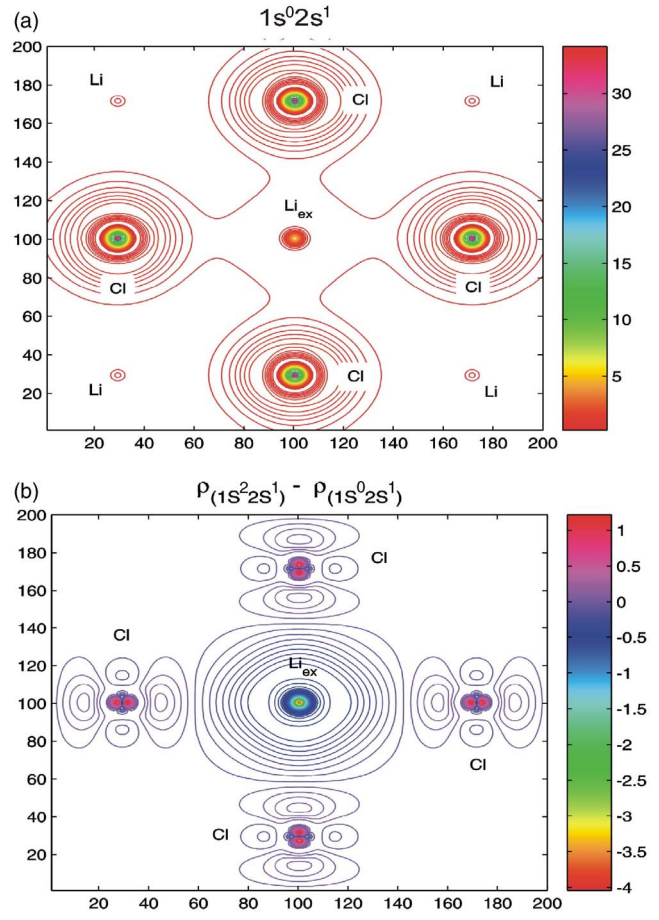

FIG. 7. (Color online) The electron density in the presence of two core holes on the central Li atom (a), and the difference compared to the ground state (b).

sity crossing the scattering map (Fig. 8) from the lower left corner, $E_1 \approx 144$ eV, $E_2 \approx 72$ eV, up to $E_1 \approx 170$ eV, $E_2 \approx 85$ eV, are due to elastically scattered radiation in second order of diffraction. These "elastic peaks" are used to calibrate the emission energy scale. Since the energy width of the exciting radiation is about 0.1 eV, the peak shape is fully governed by the spectrometer function, which hence can be directly determined. The dots also illustrate the number of measured SXE spectra per excitation energy interval, which limits the vertical energy resolution in the scattering map: in regions of sharp resonances the density of spectra is large, while at higher excitation energies we have chosen larger excitation-energy spacing, indicated by larger vertical extension of the elastic peaks. The reflectivity of the sample is dependent on the surface structure and the excitation energy. The intensity of the elastically scattered radiation markedly decreases at excitation energies above the resonance at 148 eV. The elastically scattered radiation can, however, not be directly related to the double excitations and will not be discussed further. For normalization of the SXE spectra relative to each other we rely on the measured PFY.

There are also some low-intensity features showing up as narrow horizontal lines or ridges in the background between different adjacent SXE spectra and in regions which lack emission features. These are due to uncertainties in the background, and are sensitive to normalization. They will be ignored in the following discussion.

3. Assignment of the salient features

Around 148 eV excitation energy and 84–89 eV emission energy the scattering map has an intensity maximum corresponding to the large resonance seen in PFY. This structure has two main components resonating at $E_1 \approx 148.6$ eV and $E_1 \approx 150.1$ eV. The two maxima at 148.6 and 150.1 eV ex-

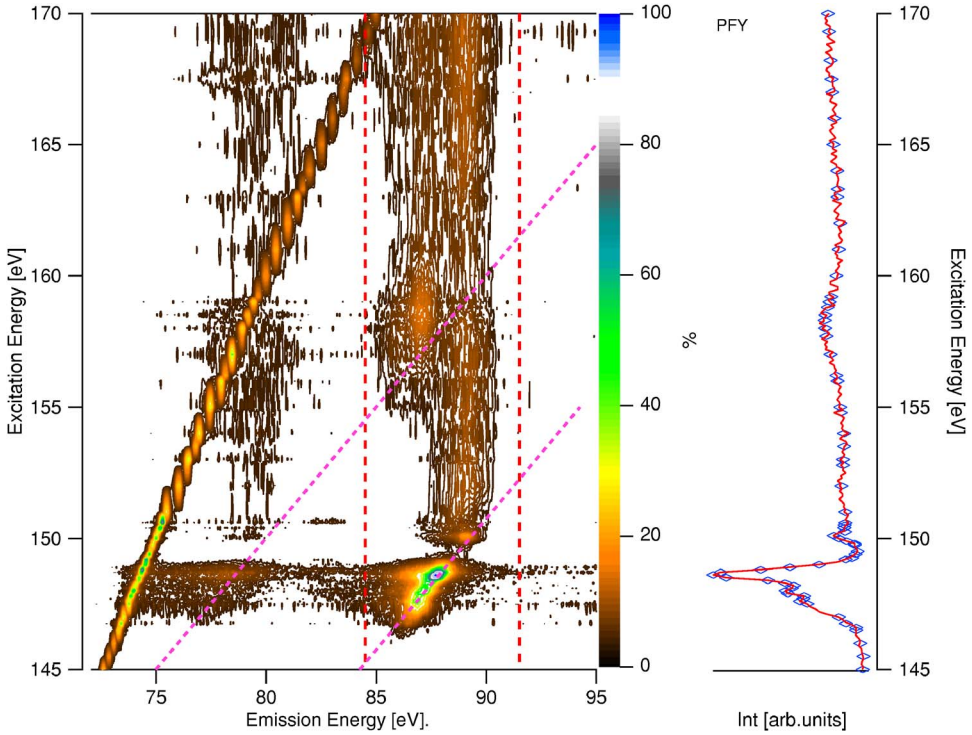

FIG. 8. (Color online) The scattering map is compiled from SXE spectra taken at 68 different excitation energies. These have been normalized to the partial fluorescence yield (PFY) shown to the right of the two-dimensional map. The diamonds in the PFY represent the integrated intensity of the emission spectra at the corresponding excitation energy. Dashed vertical lines show PFY integration area and diagonal lines show 1:1 dispersion.

citation energy are close to the $1s^2\ ^1S \rightarrow 2s2p\ ^1P$ transition in free Li^+ which is at 150.3 eV.[20,21] This makes it straightforward to assign these features to localized double excitations of the two Li 1*s* electrons. To separate the various types of excitations we use Greek letters for the first step of the scattering process and numerical subscripts for the emission step. Excitations to this type of intermediate states, in which both excited electrons are localized are denoted α.

The emission from such intermediate states is dispersing with excitation energy, indicating that similar final states are reached for all excitation energies. The energy of the emitted photon corresponds to the difference between the energy of the incoming radiation and the energy of the final state relative to the ground state. We shall see that the main energy-loss feature is very close to the excitation energy of the single core excitons in LiCl. Here we note also that the emission energies in the region of 84–89 eV are close to the $2p^2\ ^3P \rightarrow 1s2p\ ^3P$ transition in the free lithium ion at 87.9 eV,[22] and the predicted energy of the $2s2p\ ^1P \rightarrow 1s2s\ ^1S$ transition, which is at 89.3 eV.[21] The full scattering process leading to this type of final states we name α_1, and with e_L denoting an excited electron localized at the lithium site it can be written

$$\mathrm{GS} \rightarrow 1s^{-2}e_L^2 \rightarrow 1s^{-1}e_L^1 \quad (\alpha_1).$$

In Fig. 8 there is also a structure at $E_2 \approx 78$ eV for α excitation energies. This structure is located around 9 eV below the α_1 feature on the emission energy scale. The optical band gap in LiCl is 9.4 eV,[18,19] and we can therefore assign this feature to an emission process where the transfer of one of the localized electrons to one of the core holes is accompanied by the transfer of an electron from the valence to the conduction band. The feature is dispersing with the excitation energy in the same way as the α_1 emission, and is referred to as α_2 scattering. With e_{VB} and e_{CB} denoting a valence-band and conduction-band electron, respectively, the process can be written:

$$\mathrm{GS} \rightarrow 1s^{-2}e_L^2 \rightarrow 1s^{-1}e_L^1 e_{VB}^{-1} e_{CB}^1 \quad (\alpha_2).$$

Above $E_1 \approx 150.5$ eV the linear dispersion is lost, the main features shift to slightly lower energies, and as excitation energy increases to 152 eV and beyond, salient features are found at constant emission energy, $E_2 \approx 89.1$ eV. The energy region between $E_1 \approx 150.5$ eV and $E_1 \approx 152$ eV contains delocalization thresholds, above which one of the two Li 1*s* electrons delocalizes while the other is excited to a localized level. We call such a process β excitation. The excited state subsequently decays with the transfer of the localized electron to the 1*s* level, leading to final states with one core hole and one electron in the continuum. This emission process can be seen as the recombination of a core exciton in the presence of a spectator core vacancy. The full process is referred to as β_1 scattering, and it can be written

$$\mathrm{GS} \rightarrow 1s^{-2}e_L^1 e_{CB}^1 \rightarrow 1s^{-1}e_{CB}^1 \quad (\beta_1).$$

At these excitation energies a weak feature also appears at around $E_2 \approx 80$ eV, ~9 eV below the β_1 peaks. In concordance with previous assignment of α_2 scattering, this signal is assigned to a process where there is an additional band excitation in the emission step. The final states thus have one core hole, one valence hole and two electrons in the conduction band. The process is called β_2 scattering:

$$\mathrm{GS} \rightarrow 1s^{-2}e_L^1 e_{CB}^1 \rightarrow 1s^{-1}e_{VB}^{-1} e_{CB}^2 \quad (\beta_2).$$

At $E_1 \approx 158$ eV, ~9–10 eV above the α excitation, a feature appears at $E_2 \approx 87$ eV. We assign this to a triple-excitation process in which the excitation of both core electrons to localized states is accompanied by a transition of a valence electron to the conduction band (γ excitation). The excited state then decays with the transfer of one of the localized electrons to the core level, giving final states with a core exciton, and a band excitation. We refer to this process as γ_1 scattering:

$$\mathrm{GS} \rightarrow 1s^{-2}e_L^2 e_{VB}^{-1} e_{CB}^1 \rightarrow 1s^{-1}e_L^1 e_{VB}^{-1} e_{CB}^1 \quad (\gamma_1).$$

The final states are of the same type as those populated in α_2 scattering. Contrary to α_2 scattering the γ_1 feature does not disperse with excitation energy but stays at 87 eV emission energy for all excitation energies above 158 eV. This suggests that different continuum states are reached as the energy is varied in the case of γ_1 scattering, where the band excitation is created in the first step, whereas there is no such selectivity in α_2 scattering, where the valence-to-conduction-band continuum excitation takes place in the emission step of the scattering process.

C. Localized double excitations (α)

As described above, the α excitation corresponds to excitation of both lithium 1*s* electrons to states where they stay localized during the lifetime of the double core hole state. The PFY spectrum (Fig. 9) has two maxima at $E_1 \approx 148.6$ eV (*A*) and $E_1 \approx 150.1$ eV (*B*), and the former peak shows at least four visible structures, $\alpha A'''$, $\alpha A''$, $\alpha A'$, and αA, located at 147.0-, 147.5-, 148.0-, and 148.6-eV excitation energy, respectively. A four-peak Voigt fitting to the most intense peak gives a smallest width of 0.65 eV for the intense αA feature. The width of the *B* structure is about 1.6 eV, and it does not show any apparent substructure.

In the inset we compare the spectra measured with the spectrometer in the vertical and horizontal directions. There is a pronounced angular dependence; especially we find that the sharp αA resonance is more dominating relative to other structures in the vertical direction than in the horizontal. An interpretation in terms of the expected angular dependence in a free ion suggests that the sharp αA resonance must be associated more with *sp*-like excitations, whereas the $\alpha A'''$, $\alpha A''$, $\alpha A'$ resonances have larger *pd* weight. Before discussing the intermediate states in detail we turn our attention to the second step of the scattering process.

In Fig. 10, scattering spectra excited at the αA, $\alpha A'$, $\alpha A''$, $\alpha A'''$, and αB features in the PFY are shown on the final-state energy scale, derived by subtracting the emission energy from the excitation energy. The spectra are compared to the previously published Li *K*-edge SXA spectrum.[23] The main peak[18,23] in the Li *K*-absorption spectrum has been interpreted as due to a core exciton and the remaining structure in terms of *p* character in the unoccupied states. Excitonic char-

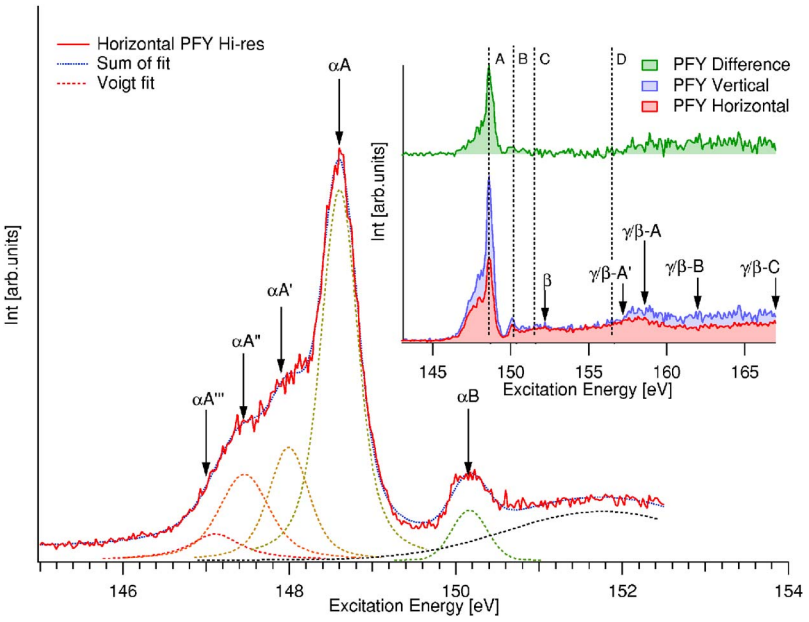

FIG. 9. (Color online) PFY spectra at the main α peak measured in the horizontal geometry. The bottom panel in the inset shows the PFY over the entire investigated energy region, measured both in the horizontal (red, in front) and vertical (blue, in the back) directions. The top panel in the inset shows the difference between vertical and horizontal PFY spectra, normalized under the assumption that intensity is always added when turning to the vertical direction from the horizontal. Arrows and labels mark excitation energies for SXE spectra which are presented and discussed in other graphs.

acter has also been attributed to the two peaks above 62 eV (Ref. 18) in the absorption spectrum. The bottom of the conduction band is situated at around 62.3 eV (Ref. 23)–62.4 eV,[24] while the continuum part of the spectrum should not gain any significant intensity until around 63.5 eV.[18,23,24]

We also show predictions of the unoccupied DOS calculated in the presence of a core hole, and projected on the Li site and angular momentum symmetries *s*, *p*, and *d*. With the excitonic character of the strongest features in the SXA spectrum, it is at first sight surprising that the local *p* DOS predicted by the supercell band calculation seems to give a fairly good representation of the spectrum. As we discussed above, however, the introduction of the core hole results in sharp localized states, due to the attractive potential. Thus part of the interactions responsible for the exciton formation is included in the supercell approach.

The emission features associated with the α excitations (Fig. 10) are almost stationary on the final-state energy scale. The main feature is always narrower than any feature in the direct absorption spectrum. The sharpest peak has a width corresponding to the instrumental resolution, and is found when the energy is tuned to the $\alpha A'''$ resonance and the spectrometer measures in the vertical direction. All the spectral variation, however, seems to occur within the most prominent feature measured in direct absorption.

The angular dependence shows that the local atomic selection rules are relevant when interpreting the spectra. Following the selection rules for the free atom, the excited electron has *d* symmetry after horizontal scattering, *p* symmetry after the direct absorption, and *s* symmetry is monitored by subtracting the scattering measured horizontally from the scattering measured in the vertical direction.

Using this quasiatomic interpretation scheme we identify sharp *s* states at 60.3 eV ($\alpha A'''$ excitation) and 61.2 eV (αB excitation). When the energy is varied between these excitations, states of the same symmetry between the sharp *s* states are also populated. At αA excitation there is also a sharp *s* maximum at 61.8 eV, i.e., at energies beyond the main exciton peak in direct absorption, corresponding to states close to the conduction-band minimum. In general, intensity shifts to higher final-state energy with increasing excitation energy. The "*d* states" seem to be spread out over a larger energy range, and the same general trend in dispersion is observed.

The observations presented in Fig. 10 imply that *s*, *p*, and *d* symmetries are represented in the whole range where the SXA spectrum has its principal intensity. This is in spite of the fact that calculations predict isolated sharp localized *s*, *p*, and *d* final states at different energies. The discrepancy is partly due to excitonic effects, which are not fully described by the theory. Furthermore, the observations strongly suggest that vibronic coupling breaks the symmetry, thereby apparently relaxing the dipole selection rules,[25,26] and hence affecting the angular dependence, a phenomenon well known in gas-phase scattering.[27,28]

Phonon coupling also introduces shifts and broadening of the spectral features. The fact that narrow states are identified when dipole allowed *s* symmetry is emphasized shows that vibronic coupling is particularly weak in the transitions corresponding to these spectral features. The identification of *d* symmetry is less certain, however, because it is based on the relatively small angular anisotropy, which could also be attributed to solid-state effects. The lack of sharp structures supports this alternative interpretation.

In the horizontal geometry in which *s* symmetry is forbidden, the intensity is smeared out over a larger energy region, suggesting that vibronic coupling is stronger, and thus that symmetry breaking may be important for populating these states. Although *d* symmetry is dipole allowed, not much density of *d* symmetry states are expected, according to the calculations.

The larger width of the features in the SXA spectrum suggests that vibronic excitations are more pronounced when the states are directly reached from the ground state than when reached in scattering over doubly excited intermediate states. This can be understood by considering that the change in extension of the wave functions when going from the

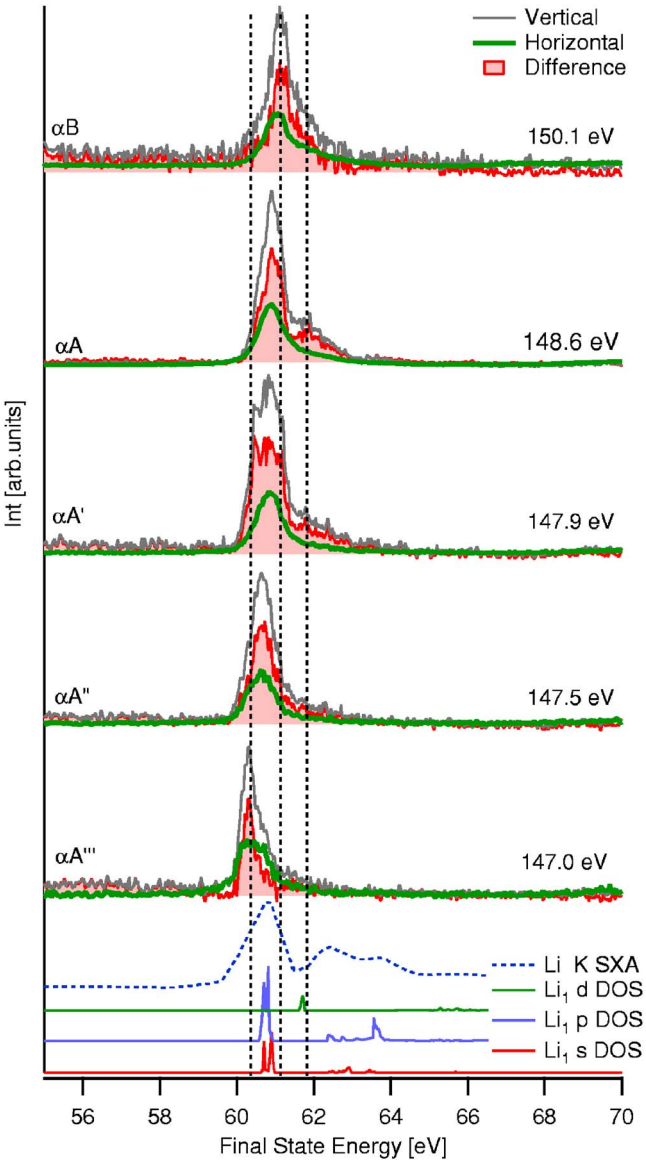

FIG. 10. (Color online) SXE spectra measured in vertical and horizontal directions, excited at the $\alpha A'''$ (147.0 eV), $\alpha A''$ (147.5 eV), $\alpha A'$ (148.0 eV), αA (148.6 eV), and αB (150.1 eV) features, and the difference between spectra measured in the two directions. The spectra are presented on the final-state energy scale. At the bottom of the graph the K-edge SXA spectrum taken from Ref. 22, and predictions of the DOS in the presence of one core hole at the central Li atom, projected on the local s, p, and d symmetries are shown.

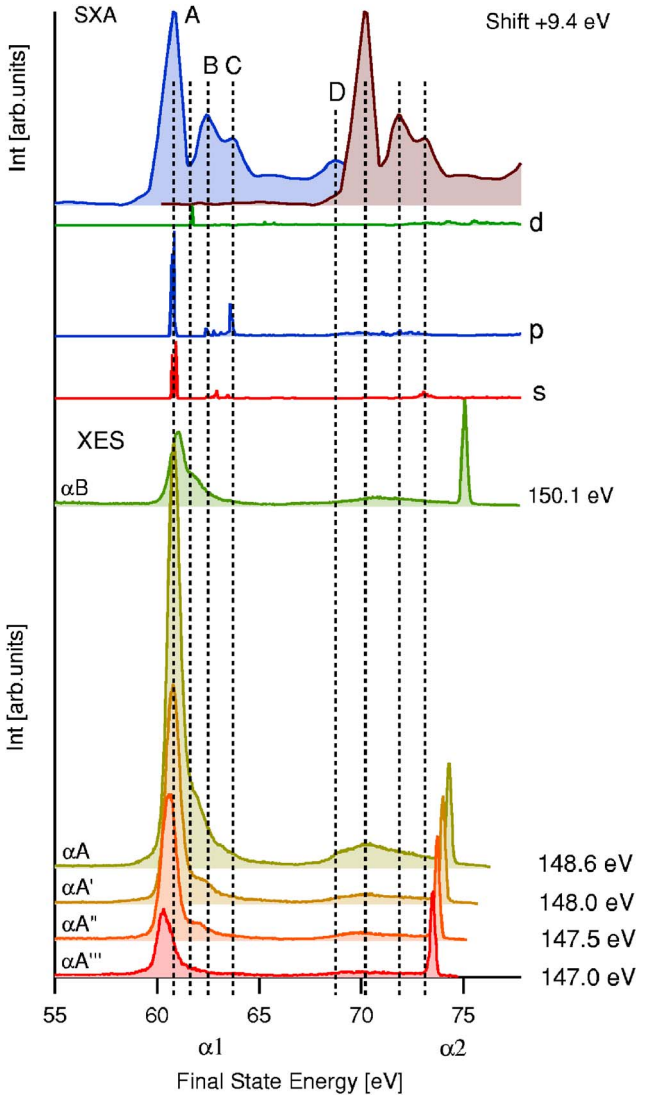

FIG. 11. (Color online) SXE spectra measured in horizontal mode shown over an extended energy range, excited at the same energies as in Fig. 10. Li K-SXA spectrum (Ref. 22) is shown in the top panel on the original energy scale and shifted by the optical band gap of 9.4 eV. The theoretical predictions are the same as in Fig. 10.

ground state to the single core excitation is much larger than when going to the doubly excited state. Therefore the bond-length change is likely to be smaller in the latter transition. Note, finally, that the situation is completely different from single-core exciton recombination in LiCl.[24] Here, the recombination line is (Stokes) shifted by about 1 eV, relative to the excitation energy, and has a width of 2 eV. The difference can largely be attributed to the different lifetimes; phonon relaxation is limited during the (relatively) short lifetime of the double core hole states.

In Fig. 11 we show the spectra measured in the horizontal direction over a larger energy range. Again, we see the shift of intensity of the α_1 feature as the excitation energy is tuned over the αA and αB resonances. With increasing excitation energy, intensity is increasingly found above the nominal ionization limit (around 62.3 eV), suggesting that local doubly excited states decay to final states with one core hole and an electron in the continuum. Such final states require that one of the localized electrons is shaken off while the other is filling one of the core holes. The process is a slightly modified α_1 scattering event:

$$\mathrm{GS} \rightarrow 1s^{-2}e_L^2 \rightarrow 1s^{-1}e_{CB}^1.$$

At higher energy losses a broad intensity maximum (α_2) is found around 70 eV. The calculations predict unoccupied states, especially of p and d symmetry in this energy region,

suggesting final states with one core hole and one electron high up in the continuum. However, the α_2 peak position coincides with the main peak of the SXA spectrum when it is *shifted* by the band-gap energy (Fig. 11). This corroborates the alternative interpretation of this feature as transitions to two-hole–two-particle final states, in which the additional energy loss compared to α_1 scattering, is attributed to an additional valence hole (principally of Cl character) and conduction-band (principally of Li character) electron. This (α_2) scattering, written $\mathrm{GS} \rightarrow 1s^{-2}e_L^2 \rightarrow 1s^{-1}e_L^1 e_{VB}^{-1} e_{CB}$, can be thought of as a "polaron" excitation in the final state, which has earlier been suggested to explain features in the absorption spectrum, in particular feature *D* in Fig. 11.[29] Below, and in a forthcoming publication where we discuss the whole series of lithium halides,[30] we will show further evidence for this interpretation.

Unlike the final states of the principal part of the α_1 scattering, the α_2 final states involve a continuum excitation, which accounts for the much larger width of the latter. From this perspective it may, however, seem surprising that both features disperse in the same way: this suggests that also in the case of α_2 scattering, the same or close-lying electronic final states are reached throughout the α resonance. This picture can be maintained by considering that both the valence band and the conduction band are rather narrow in energy.

The α_2 feature contains excitation-energy dependent internal structure, shown in more detail in Fig. 12. There is a feature at 67.4 eV (denoted $\alpha_2 B$) which is most obvious at αB excitation. Although this could also be due to a polaron excitation it does not have any counterpart in the direct absorption, and we find no straightforward assignment. A further small prepeak in the α_2 structure, found at 69.1 eV (denoted $\alpha_2 0$), lines up with the *D* peak in the unshifted SXA spectrum (see Fig. 11). It is natural to assign these features to the same final states.

To visualize the excitation-energy dependence of the discussed features we construct PFY spectra in Fig. 13, in which the final-state energy is confined according to the notation. The energy regions are labeled according to the figure caption, although due to overlapping intensity one cannot unambiguously equate a certain scattering channel with a certain energy region.

The fact that α_1I is dominating the total α PFY directly explains its similarity to the α_1I-PFY spectrum. Note, however, that all the other discussed features closely follow the α-PFY spectrum, and we can thus not find any strong selectivity in the decay channels. This is in line with the conclusion from the discussion of the angular anisotropy: all states have mixed character. There are, however, small discrepancies from the α-PFY spectrum, and we will here mention the most obvious.

The faint $\alpha_1 0$ feature does not get the same enhancement at the main resonance as the average signal, since it is so close to the α_1I feature the tail of α_1I overlaps and accounts for much of the resonant behavior of the $\alpha_1 0$-PFY signal. Thus the resonance leading to the $\alpha_1 0$ state is much less pronounced than other discussed processes. We speculate that a spin-orbit coupling in the intermediate state may change the multiplicity with a small probability and give little intensity on the low-energy side of the main peaks. A well-founded assignment of this feature, however, must await theoretical development.

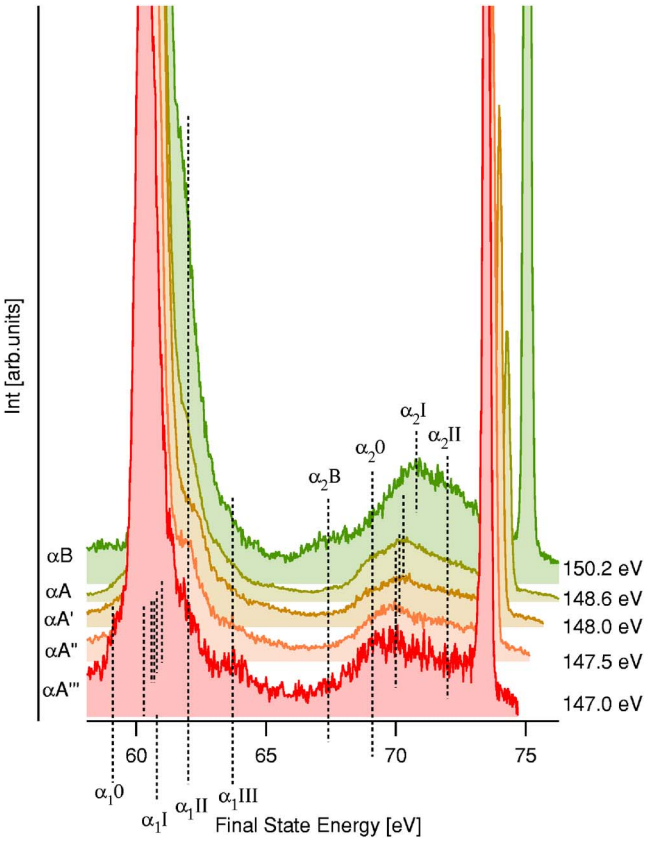

FIG. 12. (Color online) The same spectra as in Fig. 11, normalized to the α_1I integrated emission intensity, and shown on an extended intensity scale to highlight fainter structures. Substructures in α_1 and α_2 scattering are labeled for construction of PFY spectra in following figures.

The α_1II-PFY and α_1III-PFY spectra virtually coincide. The intensity is relatively smaller than in α PFY at excitation energies in the 147–148-eV excitation-energy region, and the intensity is relatively larger around and above 150 eV. The α_1II and α_1III features correspond to final states above the ionization limit, and thus the α-PFY spectra indicate that the probability of continuum excitations increase throughout the resonance.

The various α_2-PFY spectra are more similar to each other than the corresponding α_1-PFY spectra. Compared to the α-PFY spectrum, on the other hand, the main resonance in the α_2-PFY spectra are somewhat broadened at the high-energy side, and are relatively more intense above 150 eV. This suggests that also the weight of the multiparticle decay channel increases with excitation energy over the resonance.

D. Double excitations in the continuum (β)

As the excitation energy is increased beyond 150.5 eV the structures in the scattering spectra no longer remain on constant final-state energy, but rather the energy position on the emission energy scale tends to become independent of excitation energy. This is indicative of energy dissipation, and we

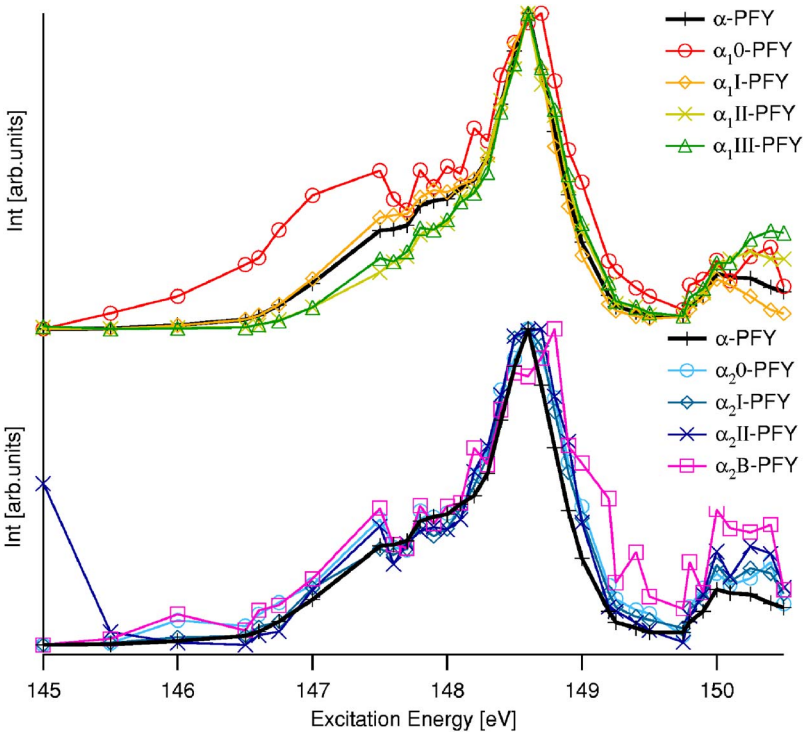

FIG. 13. (Color online) α-PFY spectra calculated from the integrated intensity in the following energy regions of the final-state energy scale, following the notation in Fig. 12: $\alpha_1$0-PFY (58.4–59.8 eV), α_1I-PFY (59.8–61.3 eV), α_1II-PFY (61.3–62.2 eV), α_1III-PFY (62.2–63.2 eV), α_2B-PFY (66.1–68.4 eV), $\alpha_2$0-PFY (68.4–69.3 eV), α_2I-PFY (69.7–71.2 eV), and α_2II-PFY (71.3–72.4 eV).

attribute this to the delocalization of one of the excited electrons from the lithium site prior to the decay of the double core hole states. Thus the intermediate states in this type of scattering (β_1) have two core holes, one localized electron and one electron in the continuum, and the final states have one core hole and one electron in the continuum: GS $\rightarrow 1s^{-2}e_L^1e_{CB} \rightarrow 1s^{-1}e_{CB}$.

First we discuss the behavior in the region between $E_1 \approx 150.5$ eV and $E_1 \approx 152$ eV, in the immediate vicinity of the delocalization thresholds. At the bottom of Fig. 14, the emission spectrum excited at 150.3 eV and measured in the horizontal direction is shown. This energy is just above the αB resonance, and we expect some contribution from transitions where both electrons are localized. At $E_1 = 150.5$ eV the spectrum is broadened to a full width at half maximum (FWHM) of 1.7 eV, while at $E_1 = 151$ eV it is again markedly narrower (FWHM ≈ 1.2 eV), and at 152.0 eV excitation energy the emission peak is again broadened (FWHM ≈ 1.5 eV). These changes are accompanied by shifts in the center of gravity, as indicated in Fig. 14. Also angular dependence shows that the spectrum has internal structure. At $E_1 = 152$ eV the low-energy part with maximum at 88.2 eV is relatively enhanced when measuring in the vertical direction, indicating that final states with the conduction-band electron in states of s character get additional weight at these energies.

The behavior in this excitation-energy region we attribute to the presence of several delocalization thresholds which are reached at slightly different excitation energies. At 151.0 eV excitation energy the small width of the peak indicates that one delocalization threshold is reached. The changes induced by increasing the energy to 152.0 eV can then be understood by overlapping emission from intermediate states with higher thresholds.

As the continuum electron is excited in the first step we assume that it does not influence the emission. The peak shape must thus reflect the intermediate state population of the localized electronic levels in the presence of two core holes. The data shows that there are several different such excitonic states, and the angular dependence shows that they have different symmetry character. We conclude that the one-electron–two-core-hole excitonic states significantly differ due to the angular momentum symmetry of the outer electron.

The total width of the β_1 scattering is significantly smaller than the nonresonantly excited one-core-hole–one-electron exciton recombination peak (FWHM=2 eV),[24] which analogously should map the intermediate state population of the localized electronic levels in the presence of *one* core hole. The reason for the discrepancy may be that for the double excitations there is no coupling to a core electron, which may influence the shape of the single core exciton. Obviously, vibrational excitations also have a large influence on the line shapes. As indicated already by the dispersion of the α resonances, vibronic coupling is less pronounced for the doubly excited states, in line with the observation of the relatively narrow β_1 lines.

E. Triple excitations (γ)

Above 154 eV excitation energy a qualitatively different feature appears at around 87 eV emission energy (Figs. 8 and 15). We attribute this to a scattering process in which three electrons are excited by the photon in the first step: the two lithium $1s$ electrons are excited to localized states, and simultaneously a band electron is promoted across the band gap. In the second step, a photon is emitted as one of the localized electrons returns to the $1s$ orbital: GS $\rightarrow 1s^{-2}e_L^2e_{VB}^{-1}e_{CB} \rightarrow 1s^{-1}e_L^1e_{VB}^{-1}e_{CB}$.

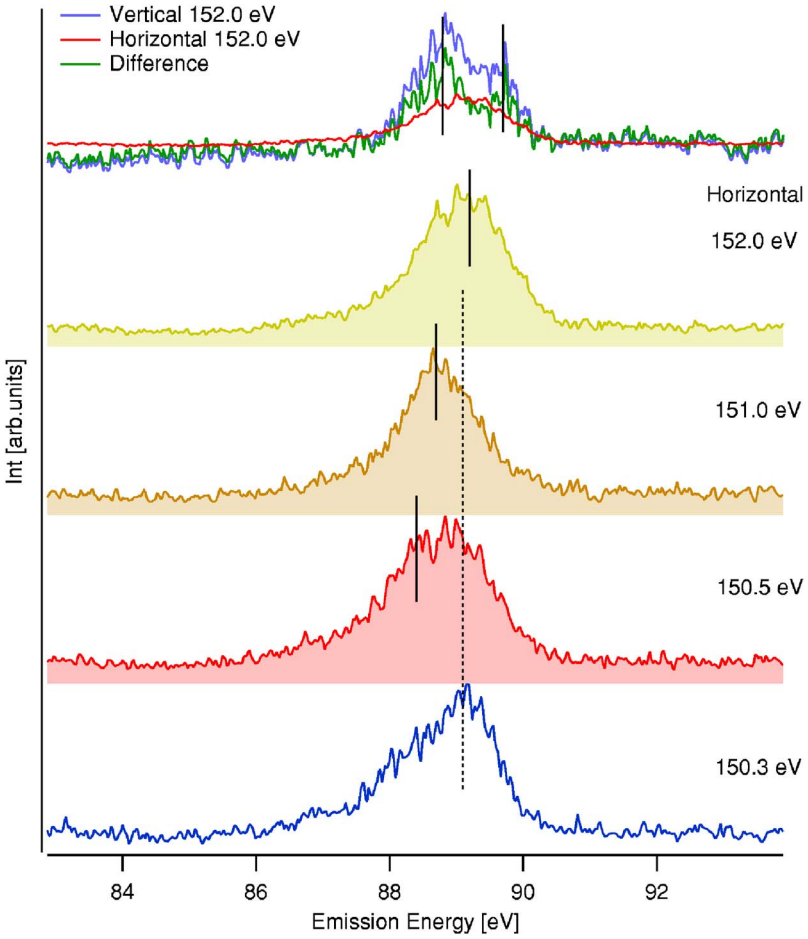

FIG. 14. (Color online) SXE spectra excited in the delocalization region. The difference spectrum is constructed under the assumption that rotating from horizontal to vertical necessarily adds intensity.

A large part of the −2 eV emission energy shift of this (γ_1) feature, relative to the β_1 feature can be understood as a simple Coulomb shift due to the local spectator electron.

The γ_1 scattering has a sharp resonance around 158 eV excitation energy, which is just above its threshold. The γ_1 emission energy is roughly constant, but its spectral shape changes markedly with excitation energy. Also here, there is a strong angular dependence, especially obvious when comparing the relative intensity of the γ_1 and β_1 features. At all excitation energies the relative γ_1 intensity is smaller when measuring in the vertical direction in which β_1 becomes totally dominating at 162 eV excitation energy and above. Pursuing the atomic angular selectivity model this implies that β_1 scattering emphasizes final states of s symmetry to a much higher degree than γ_1 scattering. For the β_1 process it is conceivable that the local partial density of states of states in the continuum for final states preferentially is of s character, thus leading to the angular anisotropy.

The final states of the γ_1 scattering are more complex and therefore any anisotropy would be more difficult to explain. A dominating isotropic contribution due to complete loss of angular momentum symmetry information, is totally in line with the observation that γ_1 intensity effectively vanishes as result of the subtraction procedure. This is the most probable interpretation of the angular dependence.

Note, however, that the observations could also be understood given final states of almost pure d symmetry, and we briefly sketch a possible scenario in accordance with such an interpretation. The final states are two-hole–two-particle core-exciton-polaron excitations with one hole in the core level, one localized electron, a valence-band hole, and a conduction-band electron. We make the ansatz that the band excitation is a monopole shake process that does not change the local symmetry. This implies that the process GS $\rightarrow 1s^{-2}e_L^2e_{VB}^{-1}e_{CB} \rightarrow 1s^{-1}e_L^1e_{VB}^{-1}e_{CB}$ only populates states where the e_L electron in the final state has d symmetry. Maintaining the atomic picture this implies that the two local electrons in the intermediate state principally have p and d symmetry, which leads to the notion that it is primarily pd double core excitons which are accompanied by a band excitation. Note also that for free ions the difference between $2l2l'$ and $2l3l'$ states is roughly 9 eV,[20] almost coinciding with the band gap in LiCl. This brings in the possibility of mixing with direct $2p3d$-like excitations, which would be situated far up in the continuum. For the helium atom the corresponding excitation has the largest scattering cross section in the radiative channel.[31,32]

Spectra measured in the horizontal direction are shown over a large emission energy range in Fig. 16. At the bottom of the graph the β_1 emission, excited at 152.2 eV, is shown. The spectral shape corresponding to the β_1 emission in the other SXE spectra, excited at higher excitation energies does not change appreciably as the excitation energy is increased, indicating constant relative population of the intermediate states as a function of excitation energy. Therefore this feature can be fitted with the β_1 emission excited at 152.2 eV,

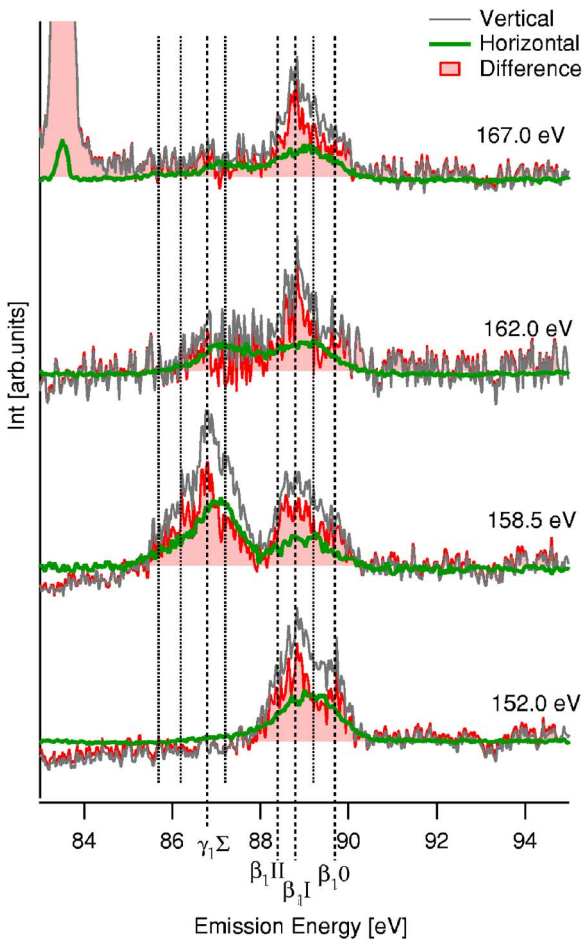

FIG. 15. (Color online) SXE spectra measured in vertical and horizontal direction for excitation energies corresponding to β and γ excitations. Difference spectra are constructed, assuming that turning from horizontal to vertical must add intensity. Labels indicate features which appear in the difference spectra, and unlabeled lines indicate structures in the horizontally measured spectrum.

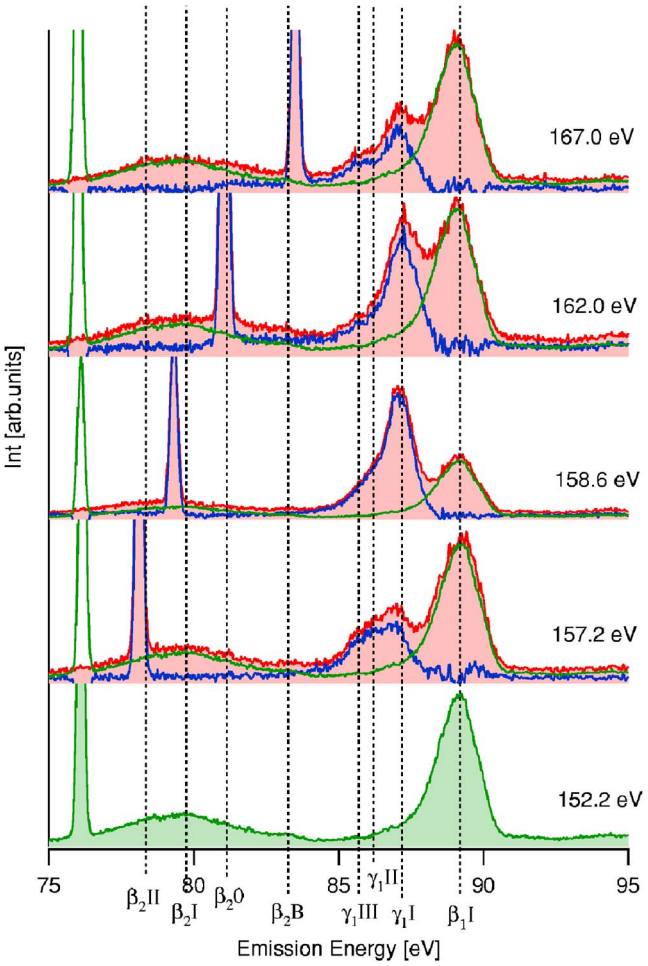

FIG. 16. (Color online) SXE spectra excited in the β and γ regions measured in the horizontal direction. The 152.2-eV β_1 spectrum (green line) has been subtracted from the original SXE spectra (red line) to get the residual spectra (blue line).

and it can be subtracted to highlight the residual γ_1 emission. At 157.2 eV excitation energy γ_1 scattering is seen as a broad structure, and as the excitation energy increases a rather sharp peak develops with maximum at 87.1 eV emission energy, and a low-energy shoulder comprising at least two substructures at 86.2 and 85.7 eV. The γ_1 emission is similar in spectral shape to the α_1 scattering. This is not surprising since in γ_1 emission a similar core excited state as in α_1 scattering decays, in the presence of a spectator valence hole and conduction-band electron.

There is also a broader structure at around 79 eV emission energy, the intensity variations of which follow β_1 rather than γ_1. We can therefore associate this (β_2) structure with the same $1s^{-2}e_Le_{CB}$ intermediate states as in β_1 scattering. The additional energy loss is due to a valence-electron–conduction-band-electron excitation in the second step of the scattering process: GS$\rightarrow 1s^{-2}e_Le_{CB}\rightarrow 1s^{-1}e_{VB}^{-1}e_{CB}^2$. The final states of this process are similar as for γ_1 and α_2 scattering, the difference being that the final state has a band electron rather than a localized electron. A close-up of the β_2 emission feature is shown in Fig. 17. Here it can be seen that there is a small change in the spectral shape with increase in excitation energy. At $E_1=150.1$ eV the β_2I feature dominates the spectral shape but at $E_1=167.0$ eV both $\beta_2$0 and β_2II have gained intensity forming a broad peak where the intensities of the different features are almost the same. It can also be noted that at the lowest excitation energy, the β_2B structure coincides with the feature identified as a_2B in Fig. 12. As it is present in SXE spectra excited at higher excitation energies (Fig. 17) this feature must be associated with delocalized intermediate β states rather than localized αB states.

In Fig. 18(a) the excitation-energy dependence of the features indicated in Fig. 16 are emphasized in PFY spectra which are constructed from the spectra shown in Fig. 8. The SXE spectra are normalized using the directly measured PFY spectrum, in which the emission energy window is set to cover the emission in the 84–92 eV range. Constructed PFY spectra for the γ_1I (86.5–87.7 eV), γ_1II (85.9–86.5 eV), and γ_1III (85.5–85.9 eV), and the β_1 (87.7–90.4 eV) emission energy regions demonstrate that whereas all the γ_1-PFY spectra show a sharp maximum around 158 eV, the rather flat β_1-PFY spectrum shows a drop in intensity at the same energy. The minimum of the β_1-PFY spectrum is, however,

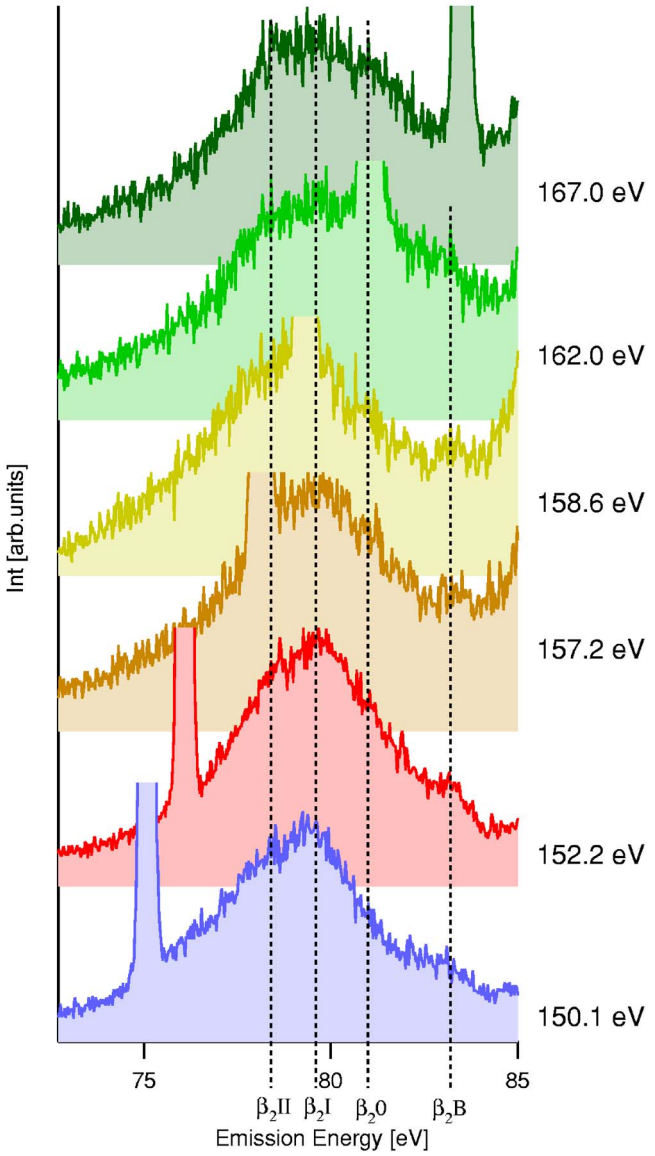

FIG. 17. (Color online) A close-up of the β_2 emission spectra excited at 152.2 eV and higher. For comparison the emission spectrum resulting from α excitations at 150.1 eV is shown at the bottom of the figure as a dashed field.

at slightly higher excitation energy than the maximum of the γ_1-PFY spectra.

Such a behavior suggests an interference effect, in which two different intermediate states reach the same final state in the scattering process. The corresponding excitation energies are sufficient to excite states in which only one electron still is localized, and the other goes into the continuum, with an accompanying valence-to-conduction-band excitation. This suggest the scattering process

$$\mathrm{GS} \rightarrow 1s^{-2}e_L^1 e_{VB}^{-1} e_{CB}^2 \rightarrow 1s^{-1} e_{VB}^{-1} e_{CB}^2 \quad (\delta).$$

As there is no local spectator electron we expect the emission energy to be similar as for β_1 scattering. This would lead to final states of the same energy as the ones reached in β_1 scattering, $1s^{-1}e_{CB}$. To account for an interference between these two channels one has to go beyond a single-configuration description of the final state, suggesting wave functions of the type $a|1s^{-1}e_{CB}\rangle + b|1s^{-1}e_{VB}^{-1}e_{CB}^2\rangle$ in the configuration interaction language. This type of interference mechanism is a suggestion on how to account for the observations. Further theoretical development is needed to be conclusive on this point.

With our assignment α_2 $(\mathrm{GS} \rightarrow 1s^{-2}e_L^2 \rightarrow 1s^{-1}e_L^1 e_{VB}^{-1} e_{CB})$ and γ_1 $(\mathrm{GS} \rightarrow 1s^{-2}e_L^2 e_{VB}^{-1} e_{CB} \rightarrow 1s^{-1}e_L^1 e_{VB}^{-1} e_{CB})$ scattering have the same final states, also when maintaining the one-electron picture. The large energy difference between the intermediate state resonances makes it difficult to observe any interference effects. On the contrary, this large difference makes it feasible to rely on the two-step approximation. Hence the principal difference between the two processes is that the band excitation occurs in the first step (γ_1) or the second step (α_2) of the scattering process. To monitor the effect of the band excitation we compare γ-PFY spectra with emission spectra excited on the α resonance in Fig. 19. The spectra are shown on an energy-loss scale which is offset by 148.6 eV for the γ-PFY spectra, and by 60.8 eV for the emission spectra, these offset energies corresponding to the simple GS $\rightarrow 1s^{-2}e_L^2$ excitation and the $\mathrm{GS} \rightarrow 1s^{-2}e_L^2 \rightarrow 1s^{-1}e_L^1$ scattering final-state energy, respectively. The agreement is excellent, strongly supporting our assignment, and demonstrating that the properties of the valence- and conduction-band states are essential for these excitations. This also implies that these properties are little influenced by whether there is a local core or a local double core excitation. Even the ratio of α_2 to α_1 is about the same as γ_1 to α_1 on the resonance, about 30%. This indicates that the probability for an accompanying band transition is about the same in the excitation stage as in the emission process. We believe that this is due to efficient screening of the core vacancies by the local electrons.

The peak position in the γ_1-PFY spectra differs somewhat [Fig. 18(b)], so that γ_1I, γ_1II, and γ_1III PFY peaks have their maximum at 158.5, 158.0, and 157.7 eV, respectively. The width of the resonances is around ~3 eV for the γ_1I and γ_1II PFY, while it is about 3.5 eV for γ_1III PFY. The small differences in excitation-energy dependence indicate that more than one triply excited state is active. This is reasonable, as we know from the analysis of the α resonance that several different doubly excited cores are possible.

In Fig. 19 we show the constructed γ_1I, γ_1I, and γ_1III PFY spectra together with the a_2 scattering spectra excited on the $\alpha A'''$, αA, and αB resonances. To facilitate the comparison of the accompanying valence excitations the main peak energies for the singly and doubly excited states, 60.8 and 148.6 eV, respectively, have been subtracted so that excess energy losses are monitored. The spectra correspond remarkably well to each other. We conclude that larger energy losses in the accompanying valence-to-conduction-band excitation are favored when the excitation energy increases both when the excitation occurs in the first and the second step of the scattering process.

Finally, we note that for the γ scattering there are no apparent features 9.4 eV below the main peak on the emission energy scale, i.e., we do not find any counterpart to α_2 and β_2 scattering. This would have implied $\mathrm{GS} \rightarrow 1s^{-2}e_L^2 e_{VB}^{-1} e_{CB} \rightarrow 1s^{-1}e_L^1 e_{VB}^{-2} e_{CB}^2$ processes, and thus scat-

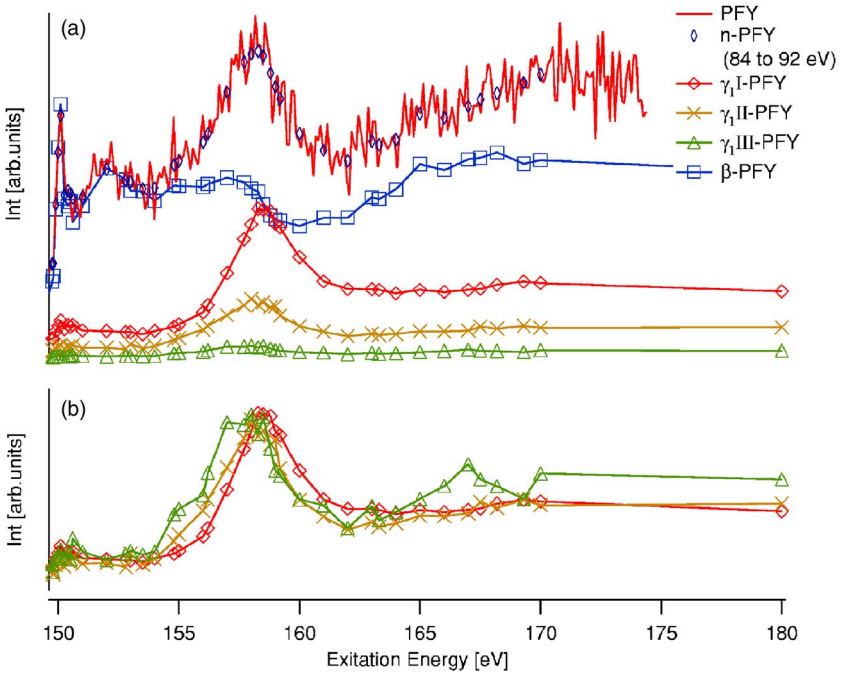

FIG. 18. (Color online) (a) PFY spectra covering emission ranges corresponding to γ_1I (86.5–87.7 eV), γ_1II (85.9–86.5 eV), and γ_1III (85.5–85.9 eV), and the β_1 (87.7–90.4 eV) emission as well as the measured total PFY between 84 and 92 eV. The β and γ PFY are plotted on the same scale, the measured PFY is normalized to fit the β_1 PFY. The diamonds in the measured PFY indicate the integrated intensity of the SXE spectra in this excitation energy range. (b) The same γ-PFY spectra as in (a) but normalized on the peak value.

tering to final states, with two valence holes and two conduction-band electrons. We expect that the cross section for such processes is small simply on the basis of the low electron density in the vicinity of the Li site.

F. Towards a theoretical description of the double core resonances

An accurate theoretical description of the localized doubly excited states is beyond the scope of this paper, which we hope will stimulate theoretical activity. The challenge is to properly account for the quasiatomic correlation between the two excited electrons, and simultaneously take the solid-state effects into account.

Here we show the predictions of a simple model, based on the LDA calculations, along the lines of which we suggested in our earlier publication.[7] There we assumed that one of the electrons prevail in a well-defined excitonic state while the other maps out the localized conduction-band states. Since the excitonic electron effectively screens one of the core holes we compared the experimental data to the DOS in the presence of one core hole. Here we note (Sec. IV A) that theoretically the screening of the two core holes partially is accounted for in the calculations. With this in mind we assume that one of the excited electrons is found in the *occupied* DOS in the presence of two core holes, and the other in the unoccupied DOS; therefore we compare the experimental

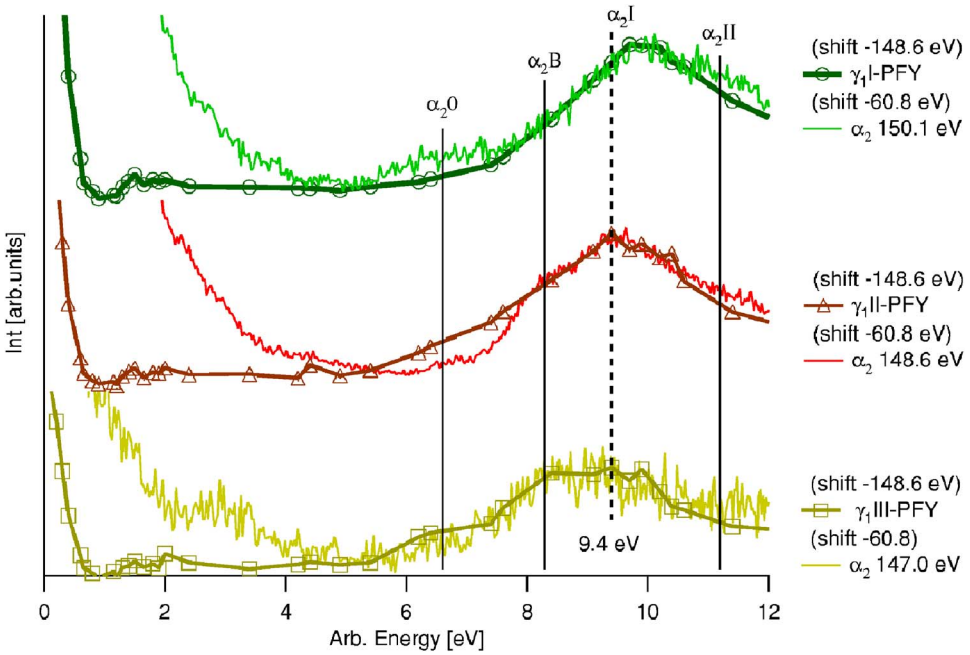

FIG. 19. (Color online) A comparison between the γ_1I, γ_1II, and γ_1III PFY spectra, and α_2 emission spectra excited at 147.0($\alpha A'''$), 148.6(αA), and 150.1 eV (αB) excitation energies. The emission spectra are plotted on the final energy scale and then shifted with the SXA-*A* energy of 60.8 eV. The γ PFY spectra have been shifted with the αA energy of 148.6 eV.

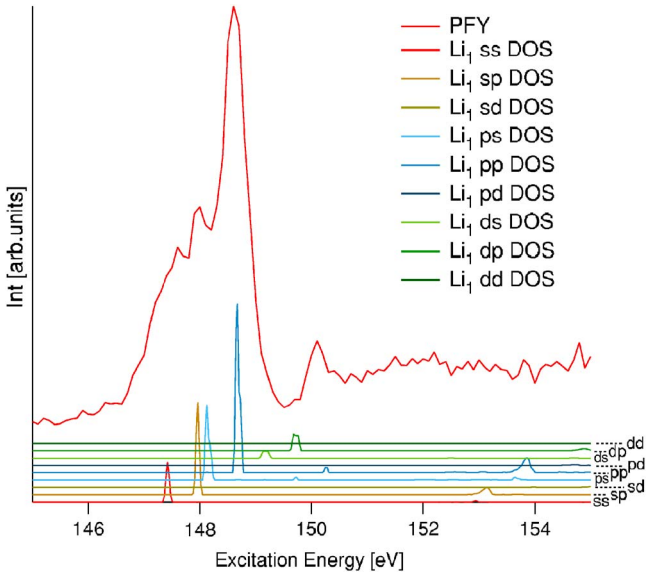

FIG. 20. (Color online) A convolution of the occupied and empty DOS in the presence of two core holes is compared to the measured PFY over the main lithium double core hole resonance.

spectra in Fig. 20 to a convolution of the occupied and unoccupied DOS in the presence of two core holes. In this convolution it is required that primary energy is shared between the two electrons so that the sum always agrees with the incoming energy.

The agreement between the predictions of this crude model and the experimental data is remarkable. Note, however, that the implied symmetry assignment disagrees with the found angular anisotropy. The model is not expected to be accurate. We hope, however, that it can inspire further development.

V. CONCLUSION

The rich phenomenology associated with RIXS at the Li double core hole states in LiCl has been presented and discussed. Several different types of multiply excited states have been identified and characterized by monioring the radiative decay channel, using both energy and angular dependence, as well as predictions based on LDA calculations. Also excitation-emission dynamics has been addressed.

We have shown that there is a wealth of spectral detail related both to the chemical state and ultrafast dynamics. Hence the excitations have a large potential for use in chemical analysis. This is further demonstrated in a systematic investigation of the lithium halide series, LiF, LiBr, and LiI,[30] and we have also observed similar excitations in molecular solids such as Li_2CO_3, Li_2O, and $LiBF_4$.[33] To take full advantage of these excitations in chemical analysis, however, a proper theoretical description is prerequisite.

ACKNOWLEDGMENTS

The authors gratefully acknowledge the support from the Swedish Research Council, the Swedish Foundation for Strategic Research, and the Göran Gustafsson Foundation. One of the authors (M.M.) wishes to acknowledge the Spanish Ministry of Science and Technology (MCyT) for financial support through the "Ramón y Cajal" program.

[1] E. T. Kennedy, Phys. Scr. **T95**, 32 (2001).
[2] N. Vaeck, J. E. Hansen, P. Palmeri, P. Quinet, N. Zitane, M. Godefroid, S. Fritzsche, and N. Kylstra, Phys. Scr. **T95**, 68 (2001).
[3] J. P. Briand, L. de Billy, P. Charles, S. Essabaa, P. Briand, R. Geller, J. P. Desclaux, S. Bliman, and C. Ristori, Phys. Rev. A **43**, 565 (1991).
[4] T. Åberg, J. P. Briand, P. Chevallier, A. Chetioui, J. P. Rozet, M. Tavernier, and A. Touati, J. Phys. B **9**, 2815 (1976).
[5] R. Diamant, S. Huotari, K. Hämäläinen, C. C. Kao, and M. Deutsch, Phys. Rev. Lett. **84**, 3278 (2000).
[6] R. Diamant, S. Huotari, K. Hämäläinen, R. Sharon, C. C. Kao, and M. Deutsch, Phys. Rev. Lett. **91**, 193001 (2003).
[7] M. Agåker, J. Söderström, T. Käämbre, C. Glover, L. Gridneva, T. Schmitt, A. Augustsson, M. Mattesini, R. Ahuja, and J.-E. Rubensson, Phys. Rev. Lett. **93**, 016404 (2004).
[8] R. Denecke, P. Väterlein, M. Bässler, N. Wassdahl, S. Butorin, A. Nilsson, J.-E. Rubensson, J. Nordgren, N. Mårtensson, and R. Nyholm, J. Electron Spectrosc. Relat. Phenom. **101–103**, 971 (1991).
[9] J. Nordgren, G. Bray, S. Cramm, R. Nyholm, J.-E. Rubensson, and N. Wassdahl, Rev. Sci. Instrum. **60**, 1690 (1989).
[10] Vienna *ab initio* simulation program developed at the Institut für Theoretische Physik of the Technische Universität Wien; G. Kresse and J. Furthmüller, Phys. Rev. B **54**, 11169 (1996).
[11] J. P. Perdew and Y. Wang, Phys. Rev. B **45**, 13244 (1992).
[12] P. E. Blöchl, Phys. Rev. B **50**, 17953 (1994).
[13] P. Blaha, K. Schwarz, G. K. H. Madsen, D. Kvasnicka, and J. Luitz, WIEN2K, an augmented plane wave plus local orbitals program for calculating crystal properties (Vienna University of Technology, Austria, 2001).
[14] W. Kohn and L. J. Sham, Phys. Rev. **140**, A1133 (1965); P. Honenberg and W. Kohn, Phys. Rev. **136**, B864 (1964).
[15] E. Sjöstedt, L. Nordström, and D. J. Singh, Solid State Commun. **114**, 15 (2000).
[16] M. Zitnik, K. Bucar, M. Stuhec, F. Penent, R. I. Hall, and P. Lablanquie, Phys. Rev. A **65**, 032520 (2002).
[17] J. Söderström, M. Agåker, A. Zimina, R. Feifel, S. Eisebitt, R. Follath, G. Reichardt, O. Schwarzkopf, J.-E. Rubensson, and W. Eberhardt (unpublished).
[18] S. T. Pantelides and F. C. Brown, Phys. Rev. Lett. **33**, 298 (1974); S. T. Pantelides, Phys. Rev. B **11**, 2391 (1975).
[19] F. C. Brown, C. Gähwiller, H. Fujita, A. B. Kunz, W. Scheifley, and N. Carrera, Phys. Rev. B **2**, 2126 (1970).
[20] L. Vo Ky, P. Faucher, H. L. Zhou, A. Hibbert, Y.-Z. Qu, J.-M. Li, and F. Bely-Dubau, Phys. Rev. A **58**, 3688 (1998).
[21] L. M. Kiernan, E. T. Kennedy, J.-P. Mosnier, J. T. Costello, and B. F. Sonntag, Phys. Rev. Lett. **72**, 2359 (1994).

[22] S. Mannervik, R. T. Short, D. Sonnek, E. Träbert, G. Möller, V. Lodwig, P. H. Heckmann, J. H. Blanke, and K. Brand, Phys. Rev. A **39**, 3964 (1989).
[23] R. Haensel, C. Kunz, and B. Sonntag, Phys. Rev. Lett. **20**, 262 (1968).
[24] K. E. Miyano, D. L. Ederer, T. A. Callcott, Q.-Y Dong, J. J. Jia, L. Zhou, and D. R. Mueller, Phys. Rev. B **49**, 5929 (1994).
[25] J. R. Fields, P. C. Gibbons, and S. E. Schnatterly, Phys. Rev. Lett. **38**, 430 (1977).
[26] Y. Harada, T. Tokushima, Y. Takata, T. Takeuchi, Y. Kitajima, S. Tanaka, Y. Kayanuma, and S. Shin, Phys. Rev. Lett. **93**, 017401 (2004).
[27] P. Skytt, P. Glans, J.-H. Guo, K. Gunnelin, C. Såthe, J. Nordgren, F. Kh. Gel'mukhanov, A. Cesar, and H. Ågren, Phys. Rev. Lett. **77**, 5035 (1996).
[28] K. Gunnelin, P. Glans, J.-E. Rubensson, C. Såthe, J. Nordgren, Y. Li, F. Gel'mukhanov, and H. Ågren, Phys. Rev. Lett. **83**, 1315 (1999).
[29] See e.g., A. B. Kunz, J. T. Devreese, and T. C. Collins, J. Phys. C **5**, 3259 (1972).
[30] M. Agåker and J.-E. Rubensson (unpublished).
[31] J.-E. Rubensson, C. Såthe, S. Cramm, B. Kessler, S. Stranges, R. Richter, M. Alagia, and M. Coreno, Phys. Rev. Lett. **83**, 947 (1999).
[32] J. G. Lambourne, F. Penent, P. Lablanquie, R. I. Hall, M. Ahmad, M. Zitnik, K. Bucar, P. Hammond, S. Stranges, R. Richter, M. Alagia, and M. Coreno, J. Phys. B **36**, 4351 (2003).
[33] M. Agåker and J.-E. Rubensson (unpublished).